ARTICLE

Check for updates

Observations suggest that North African dust absorbs less solar radiation than models estimate

Adeyemi A. Adebiyi [1✉], Yue Huang[2,3,4], Bjørn H. Samset [5] & Jasper F. Kok[2]

Desert dust accounts for a large fraction of shortwave radiation absorbed by aerosols, which adds to the climate warming produced by greenhouse gases. However, it remains uncertain exactly how much shortwave radiation dust absorbs. Here, we leverage in-situ measurements of dust single-scattering albedo to constrain absorption at mid-visible wavelength by North African dust, which accounts for approximately half of the global dust. We find that climate and chemical transport models overestimate North African dust absorption aerosol optical depth (AAOD) by up to a factor of two. This occurs primarily because models overestimate the dust imaginary refractive index, the effect of which is partially masked by an under-estimation of large dust particles. Similar factors might contribute to an overestimation of AAOD retrieved by the Aerosol Robotic Network, which is commonly used to evaluate climate and chemical transport models. The overestimation of dust absorption by models could lead to substantial biases in simulated dust impacts on the Earth system, including warm biases in dust radiative effects.

---

[1] Department of Life and Environmental Sciences, University of California - Merced, Merced, CA, USA. [2] Department of Atmospheric and Oceanic Sciences, University of California-Los Angeles, Los Angeles, CA, USA. [3] NASA Goddard Institute for Space Studies, New York, NY 10025, USA. [4] Earth Institute, Columbia University, New York, NY 10025, USA. [5] CICERO Center for International Climate Research, Oslo, Norway. ✉email: aaadebiyi@ucmerced.edu

Most of the aerosol species in the atmosphere produce a cooling effect that opposes the warming effect produced by greenhouse gases[1]. However, mineral dust is one of the three main aerosol species, in addition to black carbon and brown carbon, that absorb solar radiation and therefore could add to the warming produced by greenhouse gases[1,2]. The exact amount of solar radiation that dust absorbs greatly affects its impact on the global climate system[3]. For instance, whether the net direct radiative effect of dust aerosols warms or cools the global climate system depends, in large part, on the amount of solar radiation absorbed by dust[4–6]. Therefore, determining the extent of dust absorption of solar radiation is critical to determining whether future changes in atmospheric dust will slow or accelerate the projected warming of the climate system by greenhouse gases[7]. Beyond its direct radiative impacts, dust shortwave absorption also modifies atmospheric temperature profiles, thereby altering atmospheric circulations, cloud distributions, and precipitation[8–10]. For example, enhanced dust shortwave absorption within the Saharan air layer can reduce the intensification of tropical cyclones over the North Atlantic Ocean by enhancing the low-level temperature inversion and increasing the vertical wind shear, which could ultimately weaken associated precipitation[11,12].

Despite the importance of dust shortwave absorption on weather and the climate system[13], the exact amount of shortwave radiation absorbed by dust in the atmosphere remains highly uncertain[14,15]. This uncertainty in estimating dust shortwave absorption is partially due to uncertainties in the microphysical properties of dust used in climate and chemical transport models

(Fig. 1)[13,16]. The amount of shortwave radiation absorbed by dust aerosols is quantified by the dust absorption aerosol optical depth (dust AAOD)—a parameter that depends on dust extinction, quantified by the dust aerosol optical depth (AOD), and the fraction of that extinction that is due to absorption, quantified by the single-scattering albedo (SSA; Fig. 1). Whereas global dust extinction scales with overall dust mass loading and has been effectively constrained using remote sensing observations[17–19], estimates of dust SSA remain very uncertain[13,16]. This is because dust SSA primarily depends on the dust size distribution, dust shape, and the dust mineralogical composition (characterized by dust refractive index), and all these microphysical properties are poorly constrained in climate and chemical transport models (Fig. 1). For example, recent studies have shown that dust size distributions assumed in global aerosol models overestimate the amount of fine dust particles (with diameter, $D \leq 5\,\mu m$) and greatly underestimate the amount of large or coarse dust particles ($D \geq 5\,\mu m$) in the atmosphere compared to in-situ measurements[4,20–22]. Since coarse dust absorbs more shortwave radiation than fine dust[23,24], this underestimation of coarse dust particles could bias estimates of dust AAOD in climate and chemical transport models[6,21,25]. Furthermore, a coarse irregularly-shaped dust particle absorbs more radiation than a spherical dust particle of the same volume and mineralogy, causing errors in models because of the common assumption that dust is spherical[26–28]. Another factor contributing to large uncertainties in the dust SSA is that it primarily depends on iron-bearing minerals, mainly hematite and goethite[29–32]. These minerals have substantial but poorly known spatial variabilities, differing significantly between different dust sources[33,34]. However, most climate and chemical transport models still implicitly assume an invariant mineralogical composition by using constant dust refractive index values that do not vary in space and time[35,36]. Because dust aerosols contribute more than a third of the total shortwave absorption in most climate and chemical transport models[15], therefore, large uncertainties in dust AAOD could substantially influence the overall impacts of aerosol absorption in the atmosphere.

One reason for the large uncertainties in dust shortwave absorption and the associated dust size distribution and refractive index is that these dust properties are difficult to obtain from remote-sensing observations. Because the instruments on these remote-sensing platforms cannot directly measure aerosol size distributions and refractive indices, inversion algorithms are needed to retrieve these key aerosol properties. However, these inversion algorithms are, in turn, generally underdetermined and thus require important underlying assumptions, such as the representation of dust shape[37,38], which could lead to substantial uncertainties in the retrieved absorption aerosol properties[39]. One such remote-sensing retrieval from the ground-based AErosol RObotic NETwork (AERONET) is widely used to characterize atmospheric aerosol properties and evaluate climate and chemical transport models[40]. However, previous studies have highlighted that AERONET retrievals of dust size distribution may be too fine when compared against near-coincidental aircraft-based in-situ measurements over North Africa, although these measurements are not column-integrated and thus not directly comparable[41]. In addition, comparisons between AERONET retrievals of refractive index and mineralogical analysis of dust particles measured onboard an aircraft indicated substantial differences in the estimated dust imaginary refractive index[42,43]. Therefore, uncertainties in dust size distribution and dust refractive index in both remote-sensing retrievals and model simulations have made it difficult to estimate dust shortwave absorption accurately and have introduced substantial uncertainties in estimates of dust impacts on regional and global climate systems[4,8,13,44,45].
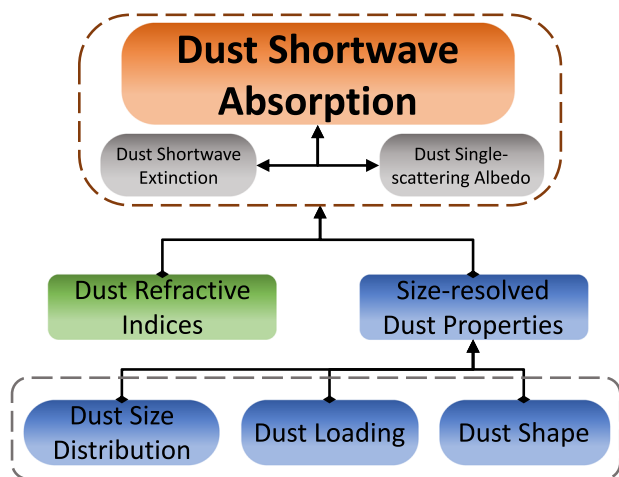

Fig. 1 Dust shortwave absorption depends on dust microphysical properties. Dust shortwave absorption—quantified by the dust absorption aerosol optical depth (dust AAOD)—depends on dust shortwave extinction and dust single-scattering albedo, both of which depend on dust microphysical properties. Direct and continuous observations of these microphysical properties, including, dust refractive index, dust size distribution, and dust shape, are difficult to obtain from remote-sensing platforms. Therefore, overall uncertainties in dust shortwave absorption depend primarily on the uncertainties in these microphysical properties. To obtain constraints on dust AAOD at 550 nm wavelength, we obtained constraints on dust refractive index in this study, which leveraged over a dozen measurements of dust single-scattering albedo at 550 nm wavelength over North Africa (green shaded box; see Methods). These constraints are then combined with observationally informed constraints on dust size distribution, dust loading, and dust shape from previously-published datasets that similarly leveraged in-situ measurements of dust properties (blue shaded boxes)[4,22,28,90] to obtain constraints on dust AAOD.

Here we address these problems by leveraging observationally based constraints on size-resolved dust properties and dust refractive index to constrain the dust shortwave absorption (Fig. 1). Specifically, we developed a framework that leveraged dozens of in-situ measurements of dust SSA to constrain the dust refractive index, which is combined with observationally based constraints on size-resolved dust properties to constrain the dust AAOD at mid-visible (550 nm) wavelength (Methods & Fig. S-1). Although dust shortwave absorption occurs across the solar spectrum, we focus on the 550 nm wavelength and use it as a representative wavelength. This is because, 550 nm wavelength is the reference wavelength used in most modeling and remote sensing studies[17,46]. Estimates of dust shortwave absorption at other visible wavelengths can be obtained by combining measurements of the spectral distribution of dust absorption properties[47,48] with our constraints at 550 nm wavelength. In addition, we focus on dust emitted from North Africa, the world's largest dust source, because it accounts for more than half of the global dust mass burden[49,50]. As such, uncertainties in the absorption properties of North African dust can substantially influence estimates of dust impacts on the global climate system[51]. Overall, our observationally based constraints suggest that North African dust absorbs substantially less shortwave radiation than estimated by an ensemble of climate and chemical transport model simulations and retrieved by the AERONET inversion algorithms. This suggests that models and retrievals might overestimate dust shortwave absorption, implying substantial biases in estimates of dust impacts on the energy balance, precipitation, and other critical aspects of the regional and global climate systems.

Results and discussion

The imaginary refractive index of North African dust. We obtained constraints on the imaginary refractive index of North African dust by leveraging more than a dozen in-situ measurements of dust single-scattering albedo (SSA) over North Africa (Figs. 1 & S-1). Specifically, we used an optimization method[52], whereby we obtained the dust imaginary refractive index at 550 nm wavelength that yields a dust SSA in optimal agreement with the collection of in-situ SSA measurements (see cyan-filled bars and circles in Fig. 2a, b, respectively, and more details in Table S-1). Our estimates of dust SSA better reproduce the compilation of in-situ measurements of dust SSA over North Africa than estimates from climate and chemical transport models (Fig. 2a). Specifically, the climate and chemical transport models consistently underestimate the dust SSA in-situ measurements at 550 nm wavelength. To put these measurements and model simulations of dust SSA on a similar footing, we calculated the simulated values over the same diameter range, height range, locations, and season as reported for the measurements (see Methods). We made the comparison of dust SSA for two sets of model simulations—an ensemble of six selected models (gray bars in Fig. 2a) and an ensemble of eight models that are part of the AeroCom (Aerosol Comparison between Observations and Models) Phase III project (dark-green bars in Fig. 2a) (see Table S-2 for details of both sets of models). We estimated mean dust SSA values of about 0.95 (standard error: 0.94–0.97) and 0.94 (standard error: 0.93–0.96) for the ensemble of selected models and AeroCom models, respectively. In contrast, the in-situ measurements revealed that North African dust generally has higher dust SSA values with a mean of about 0.97 (mean values range between 0.92 and 0.99) than the climate model simulations, over the same diameter range, height range, locations, and season. These discrepancies between the in-situ measurements and simulated dust SSA are consistent for cases with sub-micron diameter cut-off[24,53–57] and for cases that account for larger dust particles[58–60]. Overall, the underestimation of dust SSA in the

ensemble of selected models and AeroCom models can result in a mean bias of approximately −5% over some locations and collectively result in root-mean-square errors of up to a factor of two larger than our estimate of dust SSA (Fig. S-2).

Consequently, we find the imaginary refractive index that optimally reproduces the compilation of the in-situ SSA measurements of North African dust is much smaller than assumed in most climate and chemical transport models (Fig. 2c). Specifically, North African dust has a mean imaginary refractive index at 550 nm wavelength of 0.0012 (one standard error range of 0.0009–0.0016; pink/red bars in Fig. 2c). Our analysis focused on constraining the dust imaginary refractive index because dust shortwave absorption depends more sensitively on the imaginary part of the refractive index than on its real part (e.g., Fig. S-3)[16,32,61,62]. In addition, although our source-resolved constraints on dust imaginary refractive index are informed by a compilation of in-situ dust SSA measurements, they are consistent with previous lab-based measurements of imaginary refractive index from mineral soil dust[30,63,64]. For example, Di Biagio et al.[30] used parent soil samples from North Africa and found that the dust imaginary refractive index over the Sahel has a relatively larger uncertainty than the Sahara dust source region (see blue bars in Fig. 2c for interpolated values at 550 nm wavelength). In contrast, most climate model simulations ignore these regional differences in dust imaginary refractive index and assume that the refractive indices are invariant in space and time[35]. The average dust imaginary refractive index for the ensemble of selected and AeroCom models are respectively 0.0029 (standard error: 0.0014–0.0030) and 0.0026 (0.0011–0.0031) (see Table S-2). Therefore, on average, these climate and chemical transport models overestimate the imaginary refractive index of North African dust by more than a factor of two.

Consistent with these estimates in climate and chemical transport models, we also find that dust-dominated AERONET retrievals estimate a larger imaginary refractive index at 550 nm wavelength over North Africa than obtained from our observationally based constraints (compare pink/red and purple bars in Fig. 2c). Since AERONET retrievals account for both dust and non-dust aerosol species (such as smoke aerosols), we obtained dust-dominated AERONET retrievals by applying strong criteria, including using an Ångström exponent of <0.2 to discriminate the observations that predominantly contain dust aerosols from observations containing other aerosol species[47] and thereby minimizing the non-dust component in the resulting estimates (see Methods). In addition, to put the AERONET retrievals on a similar footing as our constraints and ensemble of model simulations and because of the non-linear dependence of complex refractive index on wavelength, we fit a second-order polynomial as a function of wavelength between 440 and 1020 nm to obtain interpolated values of AERONET-retrieved imaginary refractive at 550 nm wavelength[43,64,65]. We find that the dust-dominated AERONET-retrieved imaginary refractive index is ~0.0019 (0.0016–0.0021) for all of North Africa. Although the AERONET-retrieved imaginary refractive index is slightly less than the ensemble mean dust imaginary refractive index used in models, it is comparable to values used in some members of the selected and AeroCom models (see Fig. 2c and Table S-2). In addition, like most climate models, AERONET-retrieved imaginary refractive index is larger than our constraints on dust imaginary refractive index over North Africa by about 54%.

The shortwave absorption aerosol optical depth of North African dust. We find that climate models and AERONET retrievals estimate substantially more absorption of shortwave
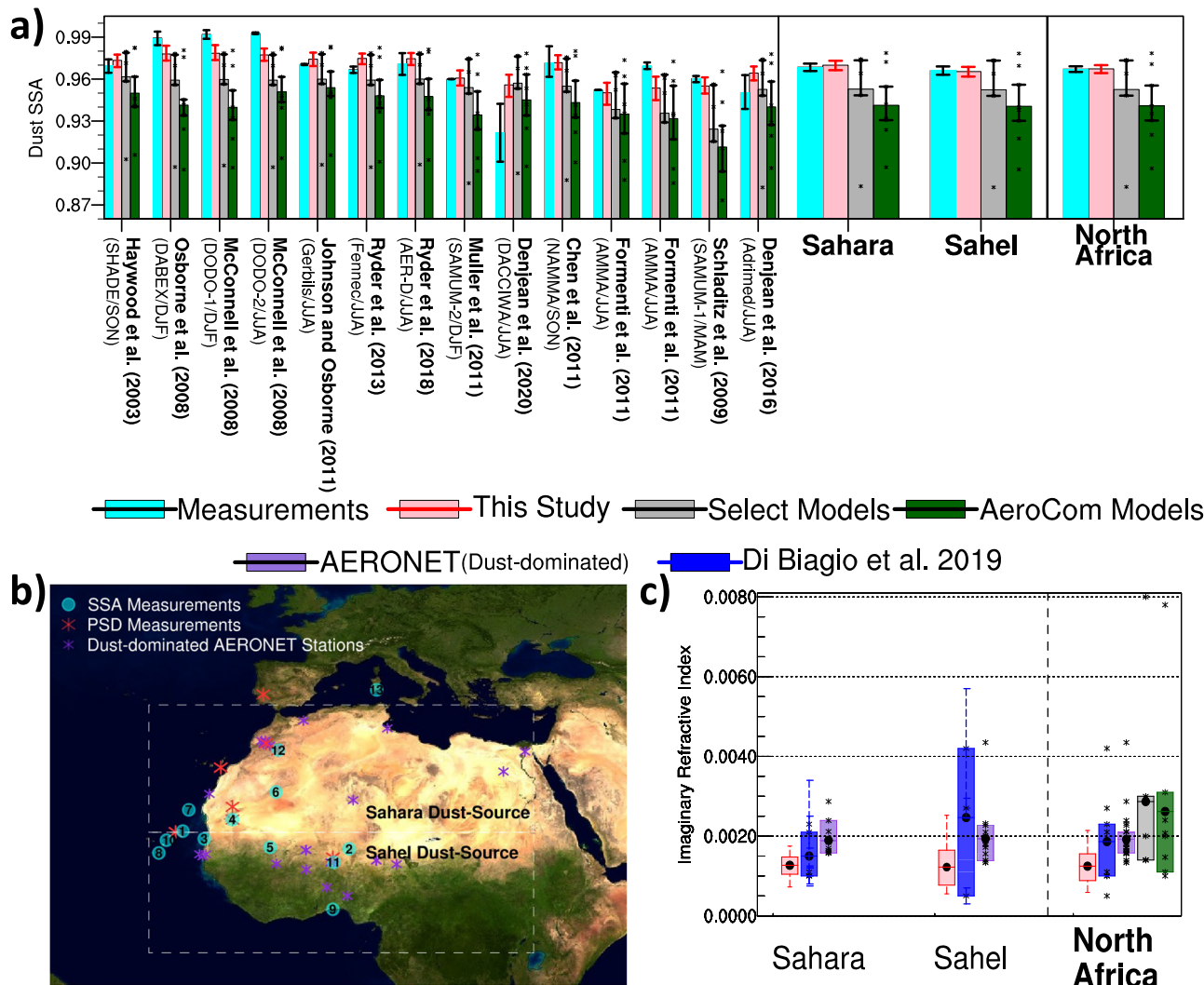
Fig. 2 Climate and chemical transport models underestimate dust single-scattering albedo and overestimate dust imaginary refractive index over North Africa. a The dust single-scattering albedo (SSA) at 550 nm wavelength obtained from in-situ measurements over North Africa (cyan bars) and the corresponding estimates from this study (pink/red bars), from an ensemble of six selected global aerosol models (gray bars), and from an ensemble of eight AeroCom Phase III models (dark-green bars; Aerosol Comparison between Observations and Models project). Details of the models that are part of the selected and AeroCom model ensembles are provided in Methods and Table S-2. The figure also includes the regionally averaged SSA at 550 nm wavelength for the Sahara and Sahel regions and for all of North Africa, as defined by the dashed boxes in Fig. 2b. The black/red vertical lines on the bars indicate the one standard error range, and the black dots represent the values from individual models in the two ensembles. **b** The locations of the 14 dust SSA in-situ measurements (cyan circles), 12 dust size distribution measurements (obtained from Adebiyi et al.[4], red stars), and 23 dust-dominated AERONET stations (purple stars; see Methods) that are used as part of this study. Details of the in-situ dust SSA measurements can be found in Table S-1 and section S-1. The boxes in (**b**) delineate the Sahara (25W–32.5E; 18–37 N) and Sahel (25W–32.5E; 0–18 N) dust source regions. **c** Comparison between the constraints on the dust imaginary refractive index at 550 nm wavelength obtained from this study (red/pink), from laboratory measurements of dust generated from several North African soil samples by Di Biagio et al.[30] (blue), and from AERONET dust-dominated observations (purple), both interpolated to 550 nm over the Sahara and Sahel regions (see Method for details). The figure also includes spatially invariant imaginary refractive index values used in an ensemble of selected global aerosol models (gray) and an ensemble of AeroCom models (dark green) at 550 nm wavelength. The box boundaries approximately indicate one standard error range; the horizontal lines and solid dots within the box denote the mean values; the red vertical lines indicate the 95% confidence interval. Finally, the stars represent the member values used in the calculation.

radiation by North African dust aerosols than indicated by our observationally based constraints. We obtained our constraints on the dust absorption aerosol optical depth (dust AAOD) at 550 nm wavelength by combining our constraints on source-resolved dust imaginary refractive index (Fig. 2c) with observationally informed constraints on dust shape[28], column-integrated dust size distribution, and dust mass loading[4,22] (see Methods). As a result, we find that the dust AAOD averaged over the North African continent is about 0.0094 (0.0073–0.0120) (Fig. 3a). However, the simulated dust AAOD values over the same area are

approximately 0.0110 (0.0064–0.0494) and 0.0180 (0.0148–0.0219) for the ensemble of selected and AeroCom models, respectively (Fig. 3b, c). Furthermore, averaging over both the continent and the ocean, where North African dust sources dominate global dust loading (by more than 80%; see the dashed black contour in Fig. 3a–c)[50], our constraint on dust AAOD is about 0.0045 (0.0035–0.0057), whereas the simulated dust AAOD values are 0.0053 (0.0030–0.0232) and 0.0090 (0.0059–0.0107) for the ensemble of selected and AeroCom models, respectively. Therefore, relative to our constraints,
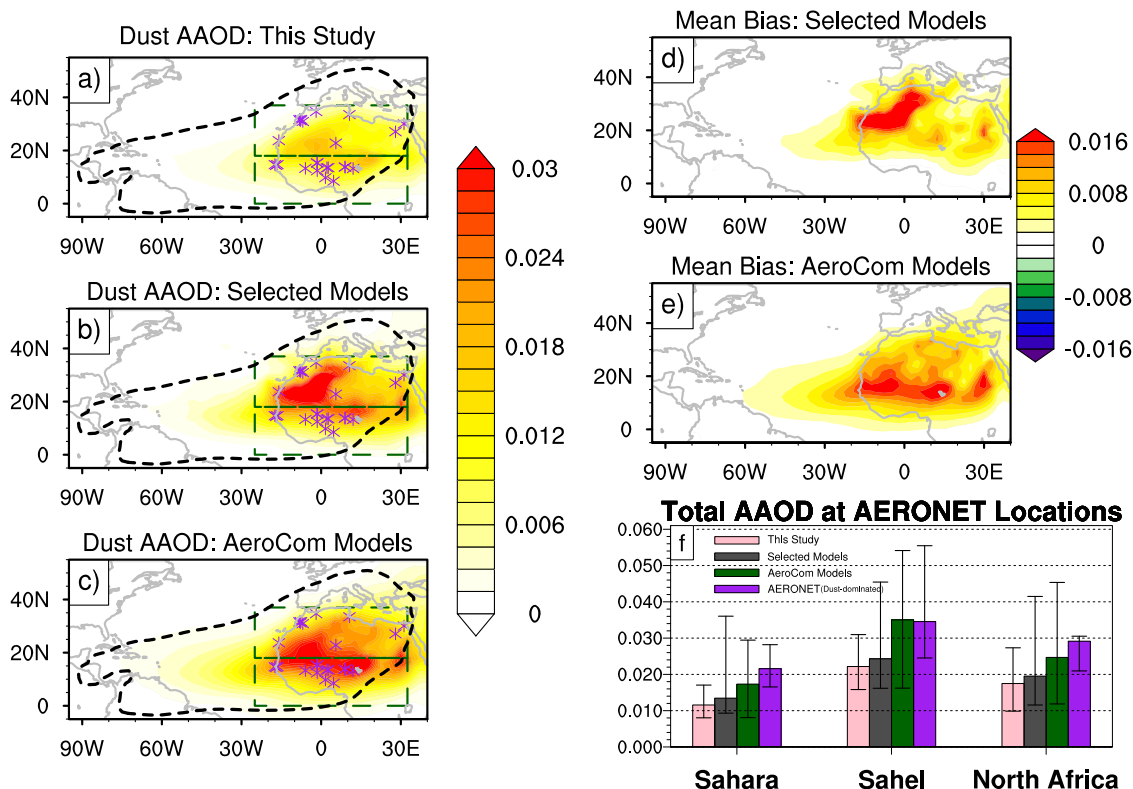
Fig. 3 Climate models overestimate dust absorption optical depth. Estimates of dust absorption optical depth (dust AAOD) obtained for (**a**) this study, (**b**) an ensemble of six selected models, and (**c**) an ensemble of eight AeroCom models. **d**, **e** The corresponding mean bias in the ensemble of selected and AeroCom models, respectively, relative to our constraints on dust AAOD. Dashed black lines in (**a–c**) delineates the region where dust emitted from North African dust sources account for more than 80% of annual dust loading[51], and the dashed green boxes delineate the Sahara and Sahel regions shown in Fig. 2b. **f** Total AAOD (dust plus non-dust AAOD) estimated at dust-dominated AERONET stations (purple stars in **a–c**), for this study (pink bars), an ensemble of selected models (dark-gray bars), an ensemble of AeroCom models (dark-green bars), and AERONET retrievals (purple bars). The total AAOD for this study and the ensemble of selected models includes the ensemble of non-dust AAOD obtained from the AeroCom models. The AERONET total AAOD minimizes the non-dust components in the resulting estimates by applying several criteria (see Methods for details). The black vertical lines on the bars denote one standard error range.

climate and chemical transport models overestimate the short-wave aerosol absorption by up to a factor of two in regions where North African dust dominates.

Similarly, we also find that dust-dominated AERONET retrievals estimate substantially greater shortwave absorption over North Africa than indicated by our observationally based constraints (Fig. 3f). As highlighted above, we use a second-order fit to interpolate to 550 nm wavelength[43,64,65] and also applied strong criteria to discriminate the AERONET retrievals that are predominantly dust aerosols and thus minimize the non-dust component in the AERONET-retrieved total AAOD (see Methods). To put the AERONET retrievals, climate model simulations, and our constraints on a similar footing, we obtained the column-integrated non-dust AAOD from the ensemble of AeroCom models and added it to our constraints on column-integrated dust AAOD. Over each AERONET station (cf. Fig. 2b), the dust-dominated retrievals are consistently larger than the total AAOD of our estimate. This possible overestimation of AAOD could reach up to a factor of three over some AERONET stations (Fig. S-4). In addition, the difference between AERONET-retrieved total AAOD and our estimates for Saharan stations is about 55% more than that for Sahelian stations (Fig. 3f). Collectively over North Africa, the average dust-dominated AERONET-retrieved total AAOD is 0.029 (0.021–0.031), whereas our estimate over the same locations is 0.017 (0.010–0.027; Fig. 3f). Although AERONET thus estimates a larger total AAOD than our constraints, the retrieved value is comparable with

model-estimated column-integrated total AAOD, which is similarly collocated with the dust-dominated North African AERONET stations (Fig. 3f). Overall, our analysis suggests that North African dust might absorb less shortwave radiation than simulated in climate and chemical transport models or obtained from dust-dominated AERONET retrievals.

The cause of possible biases in the simulated and retrieved North African dust shortwave absorption. Our observationally based constraints thus show a substantially lower shortwave absorption by dust than simulated by climate models and retrieved by AERONET. Although we cannot rule out that this difference is due to biases in the in-situ measurements of the single-scattering albedo used in our analysis, these results suggest that models and AERONET retrievals might overestimate dust shortwave absorption. To understand the cause of this possible overestimation, we decomposed the bias in dust AAOD by examining the contribution of the input parameters. Specifically, we assessed the contribution to the overall bias in the ensemble of selected models due to the bias in the simulated dust refractive index and the size-resolved dust properties, which include the dust load, dust shape, and dust size distribution (see Methods).

We find that the bias in the simulated dust AAOD is a strong function of dust diameter (Fig. 4a). Averaged over the region where North African dust sources dominate global dust loading (by more than 80%; see dashed contour in Fig. 3)[50], the ensemble of selected models overestimates dust AAOD for fine dust
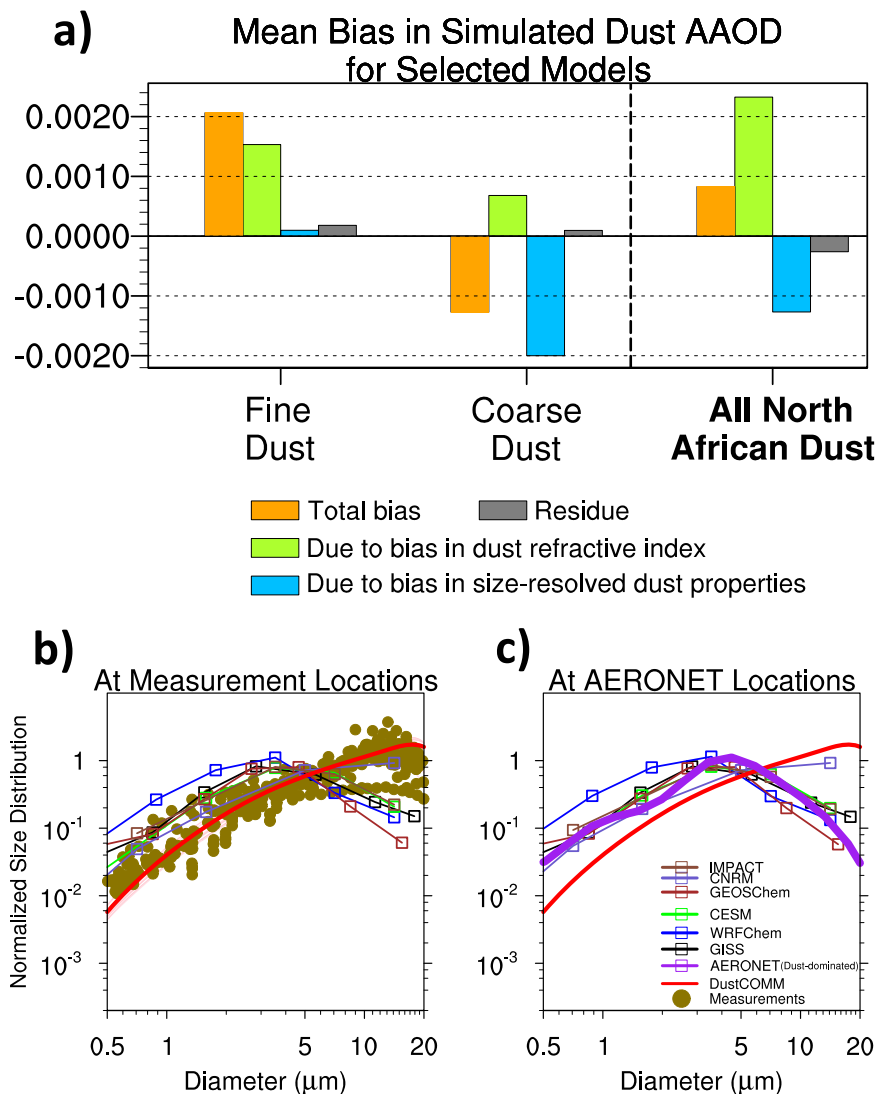
Fig. 4 The decomposition of the bias in the simulated dust aerosol absorption optical depth. a Averaged over the region where North African dust sources dominate global dust loading (by more than 80%; see dashed contour in Fig. 3)[51], the mean bias in simulated dust aerosol absorption optical depth (dust AAOD), including the total mean bias (orange bar) and the bias due to dust refractive index (green-yellow bar) and size-resolved dust properties (blue bar) which includes the biases in dust load, dust shape, and dust size distribution, obtained for the ensemble of six global aerosols models, and averaged for fine dust (diameter, $D \leq 5 \, \mu m$), coarse dust ($D \geq 5 \, \mu m$), and all dust of North African origin. The residue (gray bar) is the difference in the total bias in dust AAOD and the sum of the bias due to the bias in refractive index and size-resolved dust properties. **b, c** The normalized dust size distributions obtained from in-situ measurements (dark gold dots), collocated DustCOMM constraints on dust size distribution (red), and collocated estimates from six selected global aerosol model simulations (see Table S-1) and the aerosol size distribution obtained from AERONET retrievals (purple), compared at the locations of (**b**) the in-situ measurements and (**c**) the dust-dominated stations (see Fig. 2b) over North Africa. All size distributions are normalized between 2.5 and 10 μm (see Methods).

particles ($D \leq 5 \, \mu m$) by 0.0021 (−0.0003 to +0.0044) but underestimates it for coarse dust particles by −0.0013 (−0.0016 to −0.0009). This contrast between the overestimation of dust AAOD for fine dust and the underestimation of dust AAOD for coarse dust is primarily driven by the inherent bias in the simulated size-resolved dust mass loading. Specifically, climate and chemical transport models overestimate the fraction of fine dust particles and underestimate the fraction of coarse dust particles compared to in-situ measurements over North Africa (Fig. 4b). Depending on the model, the underestimation of coarse dust can be up to approximately one-and-a-half orders of magnitude (colored lines Fig. 4b). In contrast, DustCOMM (Dust Constraints from joint Observational-Modelling experiMental analysis), the observationally constrained dust size distribution used in this study, captures the measurements better than the

climate model simulations (compare red lines with other lines in Fig. 4b).

In addition, and across the diameter range, we also find that the bias in dust imaginary refractive index contributes a substantial fraction of the bias in the simulated dust AAOD (Fig. 4a). Specifically, the overestimation of dust imaginary refractive index in the ensemble of selected models (Fig. 2c) is primarily responsible for the overestimation of all North African dust AAOD (green bars in Fig. 4a). This contribution of the bias in dust imaginary refractive index to the bias in the dust AAOD is masked by the contribution of the bias in size-resolved dust properties, which include the size-resolved dust mass load and the shape representation. That is, the model overestimation of the fine dust load results in an overestimation of dust AAOD; the model underestimation of the coarse dust load results in an

underestimation of dust AAOD; and the spherical representation of dust shape results in an underestimation of dust AAOD. Whereas the resulting collective bias in the size-resolved dust properties results in an underestimation of the simulated North-African dust AAOD by −0.0013 (−0.0032 to +0.0054; cyan bar in Fig. 4a third column), the bias in the dust imaginary refractive index alone adds an overestimation of 0.0023 (0.0006–0.0041). Put together, the bias in the representation of simulated dust refractive index and size-resolved dust properties dust explains the majority (>70%) of the total discrepancy in the simulated dust AAOD for the ensemble of selected climate models (compare the orange and gray bars in Fig. 4a). Overall, our analysis indicates that approximately half of the model overestimation of the simulated dust AAOD due to the overestimation of the dust imaginary refractive index is offset by the model underestimation of coarse dust.

As with the ensemble of selected global aerosol models, we find that the AERONET-retrieved aerosol size distribution and imaginary refractive index explain the difference in total AAOD between dust-dominated AERONET retrievals and our estimates. Specifically, the AERONET-retrieved aerosol size distribution over dust-dominated locations overestimates fine particles ($D \leq 5\,\mu m$) and underestimates coarse particles ($D \geq 5\,\mu m$) by about the same amount as the dust size distribution in the ensemble of selected models (compare purple line with other lines in Fig. 4c). Similarly, as shown above (Fig. 2c), the AERONET-retrieved imaginary refractive index overestimates our constraints on the dust imaginary refractive index by a similar amount as the ensemble of selected and AeroCom models. These contributions from the mean aerosol size distribution and imaginary refractive index to the overestimation of retrieved AAOD are similar regardless of the Ångström exponent used to discriminate dust-dominated measurements over North Africa (Fig. S-5). This suggests that the overestimation in dust-dominated AERONET-retrieved AAOD and its associated uncertainties in the retrieved aerosol imaginary refractive index and aerosol size distribution are primarily due to the uncertainties in retrievals during dusty conditions, and for instance not due to contamination by other aerosol species. Overall, our results suggest that the possible overestimation of retrieved and simulated North African dust shortwave absorption is driven primarily by biases in dust size distribution and dust imaginary refractive index (Fig. 4).

Implications of the bias in the simulated and retrieved North African dust shortwave absorption. Our finding that climate model simulations and dust-dominated AERONET retrievals might overestimate dust shortwave absorption has important implications for dust impacts on the regional and global climate system. This is because North African dust sources emit more than half of the world's dust aerosols[49,50] and because inaccurate representations of dust absorption properties would have important consequences for our understanding of dust impacts on the global climate system[51]. One such consequence is that the bias in simulated and retrieved dust shortwave absorption could affect the estimates of regional dust direct radiative effects (DRE) with potential impacts on the global energy balance. For example, an overestimated shortwave dust imaginary refractive index (e.g., Fig. 2c) could result in a warm bias for the shortwave DRE[6,14]. However, such a bias could be masked by the contemporaneous bias in the dust size distribution (Fig. 4) since an underestimation of coarse dust by itself produces a cold bias in the shortwave DRE[4]. In addition, an underestimation of coarse dust could also introduce a cold bias in the longwave DRE[4,66], contributing to the overall bias in previous modeling studies that showed that dust cools the climate system[67–70]. Therefore, because of the sensitivity of the DRE to dust absorption properties[67,71], an accurate representation of these properties is crucial to determine whether dust warms or cools the global climate system.

Furthermore, our findings also have important consequences for our understanding of dust impacts on the hydrological cycle and biogeochemistry. Specifically, because dust shortwave absorption induces thermodynamical and dynamical responses in the atmosphere, overestimation of simulated dust AAOD could bias the temperature, moisture, and wind distribution that could, in turn, affect the distributions of clouds and precipitation[8,9,44,72]. Such effects on clouds and precipitation would depend on the vertical distribution of dust absorption properties, the ratio of fine and coarse dust particles, and the relative position of the dust and cloud layers, which climate models have found difficult to simulate accurately[25,73]. In addition, the bias in dust absorption properties could have implications for the iron mass concentration upon its deposition in the North Atlantic Ocean. Specifically, because iron-oxides are the primary mineral that controls the dust imaginary refractive index in the shortwave spectrum[30,32], our finding that models overestimate dust imaginary index of refraction implies that models likely overestimate the iron content in deposited dust particles. This inference is supported by recent studies that indicated that surface-level total iron mass concentration is overestimated near North African dust sources[74–76], suggesting that the fractional contribution of iron-oxides to total iron mass concentration is also overestimated[67]. Considering this sensitivity of the radiation budget, cloud cover, precipitation distribution, and biogeochemistry to dust absorption properties, the impacts of biases in simulated dust AAOD on the regional and global climate system could be substantial.

In addition to the consequences of the overestimation of dust absorption in climate models, our findings also have implications for retrievals of aerosol absorption properties from remotely sensed observations, particularly near dust source regions such as North Africa. Specifically, our results raise the possibility that AERONET retrievals at dust-dominated locations might overestimate the imaginary refractive index and underestimate the contribution of coarse aerosols. Such uncertainties in aerosol properties could be propagated into other applications within remote-sensing and modeling communities that utilize AERONET datasets as a benchmark. For example, most satellite-based remote-sensing retrievals rely on algorithms that often leverage AERONET retrievals of aerosol size distribution and refractive index to discriminate different aerosol types in the atmosphere[77]. One such satellite-based retrieval is from CALIPSO (Cloud-Aerosol Lidar and Infrared Pathfinder Satellite Observations), where previous studies have attributed the possible underestimation of its extinction coefficients to a bias in the dust lidar ratio, which in turn has been estimated based on AERONET retrievals of aerosol size distribution and complex refractive index[78,79]. In addition, AERONET retrievals are generally used as a benchmark with which model simulations of aerosol properties are constrained and validated[67]. For example, Bond et al.[80] adjusted the simulated direct radiative forcing of black carbon because climate models substantially underestimated AAOD when compared against AERONET retrievals (see also Fig. 3f). However, given that our results suggest that AERONET-retrieved dust-dominated AAOD might be overestimated over North Africa, such adjustments of the simulated radiative forcing could result in an overestimation of aerosol direct radiative forcing. Therefore, because of the global coverage of the AERONET stations, a more accurate constraint on the AERONET-retrieved aerosol size distribution and refractive index is crucial for the retrieval of aerosol properties from other remote-sensing platforms and to better constrain model simulations of the impacts of dust and other absorbing aerosols on key aspects of the Earth system.

Since our findings rely on in-situ dust SSA measurements and other input observational-based parameters over North Africa, it is subject to some important limitations (see Methods for details). One of these limitations includes uncertainties and biases associated with instrumentations, which may result in the dust SSA measurements not fully accounting for all the particle sizes observed over North Africa. For example, coarse and super-coarse dust particles, while present over North Africa[4,81], are often not measured by commonly-used instruments, such as nephelometers and Particle Soot Absorption Photometers[24,54,56,59]. In addition, the fine-mode size range of most of the SSA measurements is also susceptible to contamination by other aerosol species, such as black carbon, even though these measurements are obtained over dust-dominated regions[82,83]. Additional limitations to our results may be introduced through inherent uncertainties in other observationally based datasets we used as inputs, including uncertainties in the DustCOMM dust size distribution, dust loading, dust shape, and the fractional contribution of each dust source used to constrain the dust absorption properties (see Methods). For example, uncertainties may be introduced through the assumption of a representative location and height range used for dust SSA measurements (Fig. 2a), as well as the exclusion of particles larger than $D \geq 20\,\mu m$ in the DustCOMM dust size distribution. We propagate some of these uncertainties into our estimates of dust refractive index and dust AAOD by using a non-parametric procedure based on the bootstrap method[84,85] that randomly selects (with replacement) from the probability distributions of each of the input parameters (see Methods).

Because of these limitations and uncertainties, our calculated errors on dust imaginary refractive index and dust AAOD should be considered as lower bounds. This is particularly relevant for the assessment of AERONET-derived imaginary refractive index and total AAOD[86–88]. For example, in-situ dust SSA measurements used to constrain source-resolved dust imaginary refractive index are not directly collocated with AERONET dust-dominated sites, and even in locations that are collocated, in-situ measurements are obtained over specific atmospheric layers, whereas AERONET retrievals are over the entire atmospheric column. Similarly, our comparison with AERONET-retrieved total AAOD uses our constraints on dust AAOD and estimates of non-dust AAOD from an ensemble of AeroCom models. However, most models underestimate the burden of black carbon in the atmosphere, which dominates non-dust AAOD[80]. As such, the differences between our constraints and AERONET retrievals are likely smaller than indicated for dust imaginary refractive index in Fig. 2c and total AAOD in Fig. 4f. Furthermore, this suggests that the analysis cannot directly establish that our constraints are more accurate than those obtained from AERONET and that the overestimations of AERONET-retrieved imaginary index and AAOD are likely smaller over North Africa (e.g., Fig. S-5).

In conclusion, our results suggest that climate models overestimate mid-visible absorption by North African dust. Specifically, we found that the imaginary refractive index that optimally reproduces a compilation of in-situ measurements of the single-scattering albedo of North African dust is less than what is assumed in most climate and chemical transport models over North Africa. By itself, this underestimation of the imaginary refractive index relative to what is indicated by measurements would result in an overestimation of mid-visible absorption and AAOD by climate models. However, our results further suggest that this overestimation might be partially mitigated by climate models underestimating the abundance of coarse dust (dust diameter, $D \geq 5\,\mu m$) relative to in-situ measurements. In addition, our results also suggest that similar factors may contribute to an overestimation of dust-dominated total AAOD retrieved by

AERONET over the Sahara and Sahel regions of North Africa. Because approximately half of the global dust is emitted from North African sources[49,50], our finding that models and remote sensing retrievals might overestimate mid-visible absorption suggests potentially substantial biases in estimates of dust impacts on the energy balance, precipitation, biogeochemistry, and other critical aspects of the Earth system.

Methods

We constrained the spatially varying absorption optical depth (AAOD) of North African dust by combining constraints on the distribution of dust mass loading and dust mass absorption efficiency at 550 nm, both as a function of dust diameter (Fig. S-1). The size-resolved dust mass absorption efficiency and dust mass loading, in turn, depend primarily on (a) the dust size distribution, (b) dust mass loading, (c) dust shape, and (d) dust complex refractive index (Fig. 1). We thus obtained constraints on the dust AAOD by obtaining observationally informed constraints on these four key dust properties. In the next few paragraphs, we summarize the methodology and datasets used to constrain these dust properties and, therefore, the dust AAOD and then provide more detail for each step in the following sub-sections.

To obtain constraints on the key dust properties needed to estimate dust AAOD, our framework leveraged in-situ measurements of airborne dust particles over North Africa (Fig. S-1). For the first two key dust properties—the dust size distribution and dust mass loading—we used the data from DustCOMM (Dust Constraints from joint Observational-Modelling experiMental analysis). This dataset combined aircraft-based in-situ measurements of dust size distribution with satellite-based and reanalysis-derived dust properties and an ensemble of climate model simulations[4,22]. Because these constraints on the dust size distribution and dust mass loading rely on in-situ measurements, they account for the coarse dust (diameter, $D \geq 5\,\mu m$) missing from most climate model simulations[4]. In addition, the constraint on the third dust property—dust shape—leverages the measurements compilation of dust aspect ratio and height-to-width ratio from Huang et al.[28] to account for the asphericity of dust that is commonly neglected in climate model simulations[35]. For constraint on the last dust property—the dust refractive index—we leveraged more than a dozen in-situ measurements of dust single-scattering albedo (SSA) taken over North Africa (Fig. 2a). Specifically, we obtained constraints on the dust imaginary refractive index by minimizing the disagreement between the compilation of in-situ SSA measurements and our estimates of dust SSA. Our SSA estimates utilized the regionally invariant constraints on dust shape and DustCOMM constraints on dust size distribution obtained over the same location, altitude range, season, and dust diameter range as the in-situ SSA measurements. With these constraints on the dust size distribution, dust mass loading, dust shape, and dust refractive index, we obtained constraints on dust AAOD (Fig. S-1).

Furthermore, because the dust size distribution, dust mass loading, and dust refractive index depend on dust source regions, we accounted for the contribution of North African dust sources in the constraints on dust AAOD. Specifically, we divided North Africa into two major dust source regions—the Sahara and Sahel regions (Fig. 2b)[49,50,89]. Consequently, we used the observationally informed dataset obtained by Kok et al.[90] as part of DustCOMM to constrain the fractional contribution of each source region to the dust size distribution over every location. This constraint on source-resolved dust size distribution is used in our constraints on size-resolved dust mass loading, dust refractive index, and subsequently on dust AAOD.

One major strength of our constraints on dust AAOD is quantifying the associated uncertainties for each step of the analysis. Specifically, we quantified the uncertainties in dust AAOD by using a non-parametric procedure based on the bootstrap methodology[84,85]. This propagates the uncertainties in each input dataset, including the in-situ measurements, satellite-based, and reanalysis-derived dust properties, and the spread in global model simulations used in DustCOMM. In addition, we used a similar bootstrap methodology to quantify the uncertainties in our constraints on the dust imaginary refractive index. We discuss the details of the framework used to constrain dust refractive index and dust AAOD in the sub-sections below. In addition, we compared our results with the dust-dominated aerosol refractive index and AAOD retrieved from the ground-based AErosol RObotic NETwork (AERONET) and obtained from several climate and chemical transport models.

Constraints on the imaginary refractive index of North African dust at 550 nm wavelength. Dust refractive index is one of the key ingredients that determine dust AAOD (Fig. S-1). Because dust shortwave absorption depends more sensitively on the imaginary part of the refractive index than on its real part[16,32,61,62], we focused on constraining the imaginary dust refractive index. Specifically, we constrained the imaginary dust refractive index for dust from both the Sahara and Sahel source regions by determining the values of these two variables that optimally reproduced a compilation of 14 in-situ measurements of dust single-scattering albedo (SSA) over North Africa (Fig. 2a). We compiled these dust SSA measurements that used directly measured absorption and extinction coefficients from major field

campaigns taken over North Africa (see Table S-1)[24,53–60,91–93]. These directly measured dust SSA measurements contrast indirect experimental dust SSA estimates, which are usually based on Lorenz-Mie theory calculations that neglect dust asphericity (see supplementary section S-1)[94,95]. In contrast, the directly measured dust SSA requires no assumption about dust shape and often has a lower uncertainty range than the indirectly estimated dust SSA[24]. We minimized the sum of squared differences between these directly measured dust SSA estimates and our corresponding estimates of dust SSA (cyan and pink/red bars in Fig. 2a) to obtain constraints on the imaginary refractive indices (k_r) of dust particles generated by the Sahara and the Sahel source regions (pink/red bars in Fig. 2c). That is:

$$\chi^2(k_r) = \sum_{j=1}^{N_j} \left[SSA_{Measurement}^j \left(\theta_j, \phi_j, t_j \right) - SSA_{This\ Study}^j \left(\theta_j, \phi_j, t_j \right) \right]^2, \quad (1)$$

where χ^2 is the cost function to minimize, with parameter bound for imaginary refractive index at 550-nm wavelength between 10^{-4} and 10^{-2}; $SSA_{Measurement}^j$ is the jth measurement in the compilation of in-situ dust SSA with a longitude, θ_j, latitude, ϕ_j, season t_j; $N_j = 14$ is the total number of in-situ SSA measurements available (Table S-1). The second parameter on the right of Eq. 1 – $SSA_{This\ Study}^j$ – is the dust SSA calculated for the same location and season as the jth measurement (see supplementary section S-2 for details). In addition, the $SSA_{This\ Study}^j$ is estimated over the same location, altitude range and diameter range as reported for the jth measurement (see Table S-1 for details).

To estimate $SSA_{This\ Study}^j$ and therefore obtain constraints on dust imaginary refractive index (k_r), Eq. 1 requires knowledge of three additional input parameters (see supplementary section S-2). These input parameters are (1) the dust size distribution, (2) the real part of dust refractive index, and (3) dust asphericity describing dust shape. Because $SSA_{This\ Study}^j$ and k_r can vary substantially between the Sahara and Sahel dust source regions, we also accounted for the difference in the optical properties of dust generated by each of these two dust sources. Specifically, we accounted for the fractional contribution by each dust source as a function of dust diameter to the overall dust concentration at the measurement's location. This fractional contribution by each dust source region was obtained by Kok et al.[90] as part of DustCOMM, which combined observational constraints on dust properties and dust aerosol optical depth with an ensemble of global model simulations. Consequently, we obtained the source-resolved constraints on dust size distribution by multiplying the DustCOMM dust size distribution with constraints on the fractional contribution by each dust source region to the overall dust concentration (see Eqn. S-2.3). Therefore, we obtained the source-resolved constraints on dust size distribution over the same height range and diameter range as reported for the in-situ dust SSA measurements.

For the other two input parameters, we leveraged measurement-based estimates of dust real refractive index and shape distribution of dust to determine $SSA_{This\ Study}^j$. Specifically, we used the real dust refractive index, $n_r = 1.51 \pm 0.03$ (which is the same for Sahara and Sahel) obtained from lab-based measurements of dust generated from North African soil samples by Di Biagio et al.[30] (see their Table 4[30]). Because the real part of the dust refractive index has been shown to have smaller spatial and temporal variability than the imaginary part[30,59,64], we used these lab-based measurements of dust real refractive index to represent its value in the atmosphere. In addition, we accounted for dust asphericity by using the source-invariant distributions of dust aspect ratio (AR; length-to-width ratio) and height-to-width ratio (HWR) compiled by Huang et al.[28] using measurements from dozens of studies. Since the Lorenz-Mie theory used in most global models is invalid for aspherical dust particles, we obtained constraints on single-particle optical properties that incorporate the effects of dust asphericity using the single-scattering database of Meng et al.[96] (see supplementary section S-4). Therefore, with these observationally informed constraints on dust size distribution, the real refractive index, and dust asphericity, we estimated $SSA_{This\ Study}^j$ (see sections S-2 & S-3 for details) and consequently obtained constraints on the dust imaginary refractive index (k_r) by minimizing the sum of squared differences in Eq. 1. Finally, we also quantified the uncertainties in k_r using a bootstrap method[84,85] that randomly selects (with replacement) from the probability distributions of each of the input parameters (see supplementary section S-5).

Constraints on the absorption optical depth of North African dust at 550 nm wavelength. We leveraged the constraint on dust imaginary refractive index (k_r) to obtain constraints on the absorption aerosol optical depth (AAOD) for North African dust at 550 nm wavelength (Fig. S-1). Specifically, we obtained constraints on the size-resolved dust AAOD ($\hat{\tau}_{abs}$) for dust particles generated by the Sahara and Sahel source regions by obtaining constraints on column-integrated dust mass size distribution and the size-resolved dust mass absorption efficiency, which partially depends on dust refractive index (Fig. S-1). That is:

$$\frac{d\hat{\tau}_{abs}\left(\theta, \phi, t, D \right)}{dD} = \sum_{r=1}^{N_r} \widehat{\varepsilon}_{abs,asp}^r \left(n_r, k_r, AR, HWR, D \right) \cdot \frac{d\widehat{M}^r \left(\theta, \phi, t, D \right)}{dD} \quad (2)$$

where, $\widehat{\varepsilon}_{abs,asp}^r = \frac{3}{2\rho_d} \cdot \frac{\widehat{Q}_{abs,asp}(n_r, k_r, AR, HWR, D)}{D}$ is the single-particle mass absorption efficiency ($m^2\ g^{-1}$) for dust particles generated by each source region r, ($N_r = 2$, for

Sahara and Sahel source regions; see Fig. 2a). Here, we have assumed that the density of dust particles ($\rho_d = 2.5 \pm 0.2 \times 10^3 kg m^{-3}$) is independent of the dust source region, mineralogy, and dust diameter, D[4,97–99]. In addition, $\widehat{Q}_{abs,asp}^r$ is the constraint on size-resolved single-particle dust absorption efficiency that varies as a function of source region r. It is defined as the absorption cross-section of the dust particle, normalized by the projected area of a sphere ($\pi D^2/4$) with diameter D (see supplementary section S-2 & S-4). The size-resolved $\widehat{Q}_{abs,asp}^r$ and $\widehat{\varepsilon}_{abs,asp}^r$ depend on the source-invariant constraints on the dust aspect ratio (AR; length-to-width ratio) and height-to-width ratio (HWR), the lab-based measurement of dust real refractive index (n_r), and our constraints source-resolved dust imaginary refractive indices (k_r). Since the Lorenz-Mie theory used in most global models is invalid for aspherical dust particles, we obtained constraints on $\widehat{Q}_{abs,asp}^r$ (and other single-particle dust optical properties – $\widehat{Q}_{sca,asp}^r$ and $\widehat{Q}_{ext,asp}^r$) using the single-scattering database of Meng et al.[96] that incorporates the effects of dust asphericity on the dust optical property (see supplementary section S-4).

The second parameter on the right-hand side of Eq. 2 – $\frac{d\widehat{M}^r}{dD}$ – is the constraint on the contribution of each source region r to the column-integrated dust mass size distribution ($g\ m^{-3}$) at location θ, ϕ, during season t. Specifically, we obtained $\frac{d\widehat{M}^r}{dD}$ by multiplying the constraints on the column-integrated dust mass loading ($\widehat{M}_{atm}$; $g m^{-2}$) with constraints on the column-integrated dust volume size distribution per source region ($\frac{d\widehat{V}_Z^r}{dD}$). In turn, this constraint on the volume size distribution per source region ($\frac{d\widehat{V}_Z^r}{dD}$) was calculated by multiplying the DustCOMM dust volume size distribution from refs.[4,22] with constraints on the fractional contribution by each dust source region to the size-resolved dust loading obtained from Kok et al.[90] (see Eqn. S-2.3). We normalized $\frac{d\widehat{V}_Z^r}{dD}$ such that $\int_0^{D^{max}} \sum_{r=1}^{N_r} \frac{d\widehat{V}_Z^r}{dD} dD = 1$ over each location, with the upper limit of dust diameter, $D^{max} = 20\ \mu m$.

Overall, we used observationally informed constraints on dust loading, dust size distribution, dust shape, and dust refractive index to obtain our constraints on source-resolved size-resolved North African dust AAOD at 550 nm wavelength (Eq. 1 and Fig. S-1). In addition, we also quantified the uncertainties in dust AAOD using a non-parametric procedure based on the bootstrap method[84,85] that randomly selects (with replacement) from the probability distributions of each of the input parameters (see supplementary section S-5). The probability distribution of the input parameters also propagates the uncertainties in the different in-situ measurements, satellite-based and reanalysis-derived dust properties, as well as due to the spread in the global aerosol model simulations.

Dust optical properties obtained from selected models and from AeroCom models. We obtained dust absorption properties over North Africa, and the North Atlantic Ocean from two sets of global aerosol model simulations: (1) selected climate models, which include the Goddard Institute for Space Studies (GISS) ModelE general circulation model[100], the Weather Research and Forecasting model coupled with Chemistry (WRF-Chem), the Community Earth System Model (CESM)[101], Goddard Earth Observing System model coupled with Chemistry (GEOS-Chem), ARPEGE-Climate (CNRN)[102], and Integrated Massively Parallel Atmospheric Chemical Transport (IMPACT)[103] [see Table S-2 for details]; and (2) the AeroCom (Aerosol Comparison between Observations and Models) phase III models (details on the AeroCom models can be found in the references listed in Table S-2 and at https://wiki.met.no/aerocom/phase3-experiments). From these two sets of models, we obtained the following spatially-varying seasonally averaged dust properties: from the selected models, we obtained height-resolved and size-resolved dust mass loading[22], while from the AeroCom models, we obtained the column-integrated dust AAOD and total AAOD[15].

Using these variables, we calculated other dust properties that are not part of these model simulations but are required for comparisons made in this study. For example, since dust AAOD is only available for AeroCom models, we estimated the dust AAOD for the selected models using the size-resolved dust mass loading and the dust refractive index assumed in each model (see Table S-2). In addition, to compare model simulations with the in-situ dust SSA measurements, we calculated the dust SSA for the Selected and AeroCom models using each model's assumed dust refractive index and simulated dust size distribution over the same height range and diameter range as the in-situ dust SSA measurements (Table S-1). Details of the procedures to calculate the dust aerosol absorption optical depth and the dust single-scattering albedo for selected models and AeroCom models are described in supplementary section S-6.

In addition, to understand the contribution of dust imaginary refractive index and size-resolved dust properties on the overall bias in simulated dust AAOD (Fig. 4a), we replaced the input parameters in the calculation of dust AAOD (Eq. 2) for each of the six Selected models with the constraints obtained in this study (see section S-6 for details). Specifically, for the contribution of size-resolved dust properties, we replaced simulated source-resolved dust size distribution ($\frac{d\widehat{V}_{ms}^r}{dD}$; where m_s represent each Selectd model), source-resolved column-integrated dust mass load ($\widehat{M}_{m_s}^r$) by the corresponding constraints obtained from this study (that is $\frac{d\widehat{V}_Z^r}{dD}$ and $\widehat{M}_{atm}$ respectively). In addition, the spherical representation of dust shape

is replaced by an aspherical representation obtained by the measurement compilation of Huang et al.[28] of the dust aspect ratio (AR) and height-to-width ratio (HWR) used in the calculation of single-particle dust optical properties. Furthermore, for the contribution of dust imaginary refractive index, we replaced the source-invariant values assumed for each model (i.e., k^{m_S} see Table S-2) with our source-resolved estimates (k_r). We also replace the real part of the imaginary refractive index (n^{m_S}), with the lab-based estimates (n_r) from Di Biagio et al.[30]. Therefore, the difference between these mode-based estimates and our constraints shows the contribution of that the input parameter on the simulated dust AAOD. Given the non-linear, non-additive nature of this procedure and the parameters, the combined effect of contributions does not directly reproduce the overall bias, indicating that the residual is non-zero (see Fig. 4a).

Dust optical properties obtained from AERONET. We obtained aerosol absorption optical depth, size distribution, and complex refractive index from AERONET (AErosol RObotic NETwork). While details about the AERONET project, its instrumentations, and retrieval algorithm can be found in the literature[37,38], we provide here a brief overview. AERONET provides global ground-based remote-sensing observations of aerosol extinction and retrieval of other atmospheric aerosol properties[40]. Specifically, each AERONET station is equipped with an automatic sun and sky scanning radiometer that measures the direct solar intensity and almucantar sky radiance, which are used to obtain the total column aerosol optical depth for at least the four main wavelengths (including 440, 670, 870, and 1020 nm)[104]. The spectral aerosol optical depth and the spectral sky radiances, through an inversion algorithm[37,38], are used to obtain column integrated aerosol size distribution, complex index of refraction, and subsequently the single-scattering albedo (SSA) and the aerosol absorption optical depth (AAOD).

We used AERONET version-3 aerosol properties, which include substantial improvements to the retrieval algorithm compared to the previous versions. Details of these improvements in version-3 can be found in Giles et al.[105] and Sinyuk et al.[88]. The level-2.0 of version-3 datasets applies additional quality control criteria relative to the level-1.5 datasets. Specifically, level-2.0 requires the solar zenith angle to be greater than 50 degrees and the aerosol optical depth at 440 nm to be >0.4[88,105]. Because these additional quality control criteria substantially reduce the number of available measurements by excluding days with low aerosol concentration and locations farther from the major sources over North Africa, it may result in bias in the retrieved aerosol properties. To minimize this bias, we largely follow Bond et al.[80] and combined level-2.0 with the level-1.5 dataset, only using level-1.5 for days where level-2.0 is not available. Note that our approach differs slightly from Bond et al. in that we assumed that all level-1.5 data with retrievals of AOD at 440 nm less than 0.4 have corresponding valid level 2.0 AOD retrievals. This assumption does not change the conclusion presented in this study since the fraction of stations for which we used level-1.5 AAOD retrievals is small, such that the addition of these level-1.5 retrievals introduce an error in the calculated region-wide averaged dust properties over North Africa that is small compared to other errors in the analysis (see Fig. S-8).

Furthermore, since AERONET reports the total aerosol properties and does not discriminate between aerosol species, we applied additional constraints to select the stations and retrievals that are dominated by dust aerosols over North Africa. First, we selected only days with measurements that have an extinction angstrom exponent <0.2 using wavelengths of 440 and 870 nm[47,62,106] (AE ≤ 0.2). We do so because AE ≤ 0.2 better represents 'pure dust'[107], which further helps to discriminate dust from other non-dust aerosols and have enough measurements for a statistically significant analysis over North Africa. Although some previous studies have used different values of angstrom exponent (both above and below AE = 0.2) to discriminate dust from non-dust aerosols[19,106,108], our selection here does not change the conclusion presented in this study (see Fig. S-5). For example, using a lower angstrom exponent of 0.1 still results in an overestimation of AERONET-retrieved AAOD, which is still associated with higher refractive index (although less than when AE ≤ 0.2) and lower coarse dust load (although higher than when AE ≤ 0.2), when compared to our estimates over North Africa. Second, to further improve the validity of our estimates and reduce the uncertainties in the climatological averages that we compared, we required that each monthly average contains retrievable information for at least 10 days in each month, with at least 2 months of available data for the seasonal averages[80]. Third, we selected AERONET stations whose measurements are likely dominated by dust aerosols. To do so, we used MERRA-2 reanalysis aerosol properties[109] to select only stations where the percentage contribution of dust extinction to the climatological total aerosol extinction is more than 60 % (see Fig. S-6). In addition, to avoid coastal stations with substantial contamination from sea salt in the boundary layer, we used the threshold that the climatological contribution of seas-salt aerosols to the total aerosol surface concentration (which include black and organic carbons, DMS, SO2, SO4, and dust aerosols) should be <20% for each station (see Fig. S-6). Fourth, to account for the non-linearity in the spectral variation of imaginary refractive index and AAOD, we use a second order fit of the logarithm of AERONET-retrieved imaginary refractive index and AAOD versus logarithm of the wavelength to interpolate their respective values at 550 nm wavelength[43,64,65]. Finally, to put the AERONET retrievals on a similar footing with our constraints and ensemble of model simulations, we calculated the climatological average of the quality-controlled AERONET retrievals over each location.

Limitations of our methodology. Although we quantified the uncertainties in our constraints on dust imaginary refractive index (k_r Eq. 1) and dust AAOD ($\hat{\tau}_{abs}$; Eq. 2), our methodology is still subject to some important limitations. First, limitations in instrumentation resulted in a compilation of in-situ dust SSA measurements that may not adequately account for the full range of particle sizes observed over North Africa. Although airborne dust particles with a diameter larger than 50 μm have been measured over North Africa[21,24,56,83,110], most of our dust SSA measurements are taken by airborne nephelometers and Particle Soot Absorption Photometers with sub-micron diameter cut-off less than ~3 μm[24,53–57]. Only a few of the dust SSA measurements account for particles larger than 3 μm diameter (Table S-1)[58–60,92,93]. We mitigated this issue by matching the diameter range in the calculation of dust SSA ($\text{SSA}_{\text{This Study}}^j$; Eq. 1 & Eqn. S2.1) to the diameter range captured by each measurement.

The second limitation is that additional uncertainties may be introduced into our estimates through inherent uncertainties associated with our methodology and the input datasets, including uncertainties in DustCOMM dust size distribution, dust loading, and the fractional contribution of each dust source. For example, methodological uncertainties may be introduced through the representative location and height range used for dust SSA measurements. Although we used the reported location and height range, we assigned a representative location to each dust SSA measurement based on the reported locations over which the data was taken (see section S-1). In addition, to constrain dust imaginary refractive index, we used seasonally averaged DustCOMM dust size distribution that corresponds to the measurement's season. However, the dust size distribution for a representative season and location may not necessarily reflect the condition of the specific date(s) when the measurement was taken.

Furthermore, other inherent uncertainties associated with DustCOMM dust size distribution may be introduced into our analysis (Eq. 2). Specifically, although dust particles with D ≥ 20 μm have also been measured for North African dust[21,24,56,83,110], their inclusion in DustCOMM dust size distribution may result in large uncertainties because such measurements are still relatively scarce[4,22]. As a result, we also avoided such large uncertainties in our constraints on dust AAOD. In addition, most climate and chemical transport models, including those highlighted in this study, also don't account for dust with D ≥ 20 μm, and the majority have dust with a maximum diameter of 10 μm[15,111].

An additional limitation is that our constraints on dust AAOD only accounted for the contributions from Sahara and Sahel sources. However, Kok et al.[50] highlighted that the sources over the Middle East and Central Asian regions contribute to dust aerosols reaching locations over North Africa. Although this contribution is small (about 7.5%) relative to the Sahara and the Sahel regions, it could introduce non-negligible uncertainties in the source-resolved dust mass distribution and, consequently, on our constraints on dust AAOD. Furthermore, our methodology did not account for the effect of aging on the composition of dust and, consequently, the dust refractive index as it is transported from the source regions[112]. However, previous studies with in-situ measurements pointed to little changes in the optical properties of dust plumes as they are transported from North African sources[83,113], thus suggesting that the effect of aging in our estimate of dust AAOD is likely small.

Data availability
Dust absorption properties from AeroCom models are obtained from the repository at http://aerocom.met.no (last assessed on January 2020), and AERONET-retrieved aerosol absorption properties are obtained from https://aeronet.gsfc.nasa.gov (last assessed on June 2021). Previously-published datasets, such as dust properties from the selected models and DustCOMM datasets, are available through cited publications[114–116]. Our constraints on dust imaginary refractive index and dust absorption aerosol optical depth as well as the code used to obtain these datasets are publicly available at ref. [117] (https://doi.org/10.5281/zenodo.6406831).

Code availability
Code used to generate the dust single-scattering albedo, the dust imaginary refractive index and dust AAOD are available at ref. [117] (https://doi.org/10.5281/zenodo.6406831). Matlab was used for data generation, but all figures except Fig. 1 are made using National Center for Atmospheric Research (NCAR) Command Line (NCL; https://www.ncl.ucar.edu/).

References
1. Boucher, O. et al. Clouds and Aerosols. Climate Change 2013: The Physical Science Basis. *Contribution of Working Group I to the Fifth Assessment Report of the Intergovernmental Panel on Climate Change* 571–657 (2013) https://doi.org/10.1017/CBO9781107415324.016.

2. Bellouin, N. et al. Bounding Global Aerosol Radiative Forcing of Climate Change. *Rev. Geophys. Rev. Geophys.* **58**, e2019RG000660 (2020).
3. Kok, J. F. et al. Mineral dust aerosol impacts on global climate and climate change. *Nat. Rev. Earth Environ.* **4**, 71–86 (2023).
4. Adebiyi, A. A. & Kok, J. F. Climate models miss most of the coarse dust in the atmosphere. *Sci. Adv.* **6**, eaaz9507 (2020).
5. Haywood, J. M. & Shine, K. P. The effect of anthropogenic sulfate and soot aerosol on the clear sky planetary radiation budget. *Geophys. Res. Lett.* **22**, 603–606 (1995).
6. Di Biagio, C., Balkanski, Y., Albani, S., Boucher, O. & Formenti, P. Direct Radiative Effect by Mineral Dust Aerosols Constrained by New Microphysical and Spectral Optical Data. *Geophys. Res. Lett.* **47**, e2019GL086186 (2020).
7. Kok, J. F., Ward, D. S., Mahowald, N. M. & Evan, A. T. Global and regional importance of the direct dust-climate feedback. *Nat. Commun.* **9**, 241 (2018).
8. Perlwitz, J. & Miller, R. L. Cloud cover increase with increasing aerosol absorptivity: A counterexample to the conventional semidirect aerosol effect. *J. Geophys. Res.: Atmos.* **115**, 1–23 (2010).
9. Amiri-Farahani, A., Allen, J. R., Neubauer, D. & Lohmann, U. Impact of Saharan dust on North Atlantic marine stratocumulus clouds: Importance of the semidirect effect. *Atmos. Chem. Phys.* **17**, 6305–6322 (2017).
10. Huang, J., Wang, T., Wang, W., Li, Z. & Yan, H. Climate effects of dust aerosols over east asian arid and semiarid regions. *J. Geophys. Res. Atmos.* **119**, 11,398–11,416 (2014).
11. Reale, O., Lau, K. M., Da Silva, A. & Matsui, T. Impact of assimilated and interactive aerosol on tropical cyclogenesis. *Geophys. Res. Lett.* **41**, 3282–3288 (2014).
12. Dunion, J. P. & Velden, C. S. The impact of the Saharan Air Layer on Atlantic tropical cyclone activity. *Bullet. Am. Meteorol. Soc.* **85**, 353–365 (2004).
13. Samset, B. H. et al. Aerosol Absorption: Progress Towards Global and Regional Constraints. *Curr. Clim. Change Rep.* **4**, 65–83 (2018).
14. Li, L. et al. Quantifying the range of the dust direct radiative effect due to source mineralogy uncertainty. *Atmos. Chem. Phys.* **21**, 3973–4005 (2021).
15. Sand, M. et al. Aerosol absorption in global models from AeroCom phase III. *Atmos. Chem. Phys.* **21**, 15929–15947 (2021).
16. Bergstrom, R. W. et al. Spectral absorption properties of atmospheric aerosols. *Atmos. Chem. Phys.* **7**, 5937–5943 (2007).
17. Ridley, D. A., Heald, C. L., Kok, J. F. & Zhao, C. An observationally constrained estimate of global dust aerosol optical depth. *Atmos. Chem. Phys.* **16**, 15097–15117 (2016).
18. Song, Q., Zhang, Z., Yu, H., Ginoux, P. & Shen, J. Global dust optical depth climatology derived from CALIOP and MODIS aerosol retrievals on decadal timescales: regional and interannual variability. *Atmos. Chem. Phys.* **21**, 13369–13395 (2021).
19. Huneeus, N. et al. Global dust model intercomparison in AeroCom phase i. *Atmos. Chem. Phys.* **11**, 7781–7816 (2011).
20. Kok, J. F. A scaling theory for the size distribution of emitted dust aerosols suggests climate models underestimate the size of the global dust cycle. *Proc. Natl Acad. Sci.* **108**, 1016–1021 (2011).
21. Ryder, C. L. et al. Coarse and giant particles are ubiquitous in Saharan dust export regions and are radiatively significant over the Sahara. *Atmos. Chem. Phys.* **19**, 15353–15376 (2019).
22. Adebiyi, A. A. et al. Dust Constraints from joint Observational-Modelling-experiMental analysis (DustCOMM): comparison with measurements and model simulations. *Atmos. Chem. Phys.* **20**, 829–863 (2020).
23. Otto, S., Trautmann, T. & Wendisch, M. On realistic size equivalence and shape of spheroidal Saharan mineral dust particles applied in solar and thermal radiative transfer calculations. *Atmos. Chem. Phys.* **11**, 4469–4490 (2011).
24. Ryder, C. L. et al. Coarse-mode mineral dust size distributions, composition and optical properties from AER-D aircraft measurements over the tropical eastern Atlantic. *Atmos. Chem. Phys.* **18**, 17225–17257 (2018).
25. Ansmann, A. et al. Profiling of Saharan dust from the Caribbean to western Africa – Part 2: Shipborne lidar measurements versus forecasts. *Atmos. Chem. Phys.* **17**, 14987–15006 (2017).
26. Yang, P. et al. Modeling of the scattering and radiative properties of nonspherical dust-like aerosols. *J. Aerosol Sci.* **38**, 995–1014 (2007).
27. Kalashnikova, O. V. & Sokolik, I. N. Modeling the radiative properties of nonspherical soil-derived mineral aerosols. *J. Quantitative Spectros. Radiat. Transfer* **87**, 137–166 (2004).
28. Huang, Y. et al. Climate Models and Remote Sensing Retrievals Neglect Substantial Desert Dust Asphericity. *Geophys. Res. Lett.* **47**, e2019GL086592 (2020).
29. Formenti, P. et al. Dominance of goethite over hematite in iron oxides of mineral dust from Western Africa: Quantitative partitioning by X-ray absorption spectroscopy. *J. Geophys. Res.: Atmos.* **119**, 12740–12754 (2014).
30. Di Biagio, C. et al. Complex refractive indices and single-scattering albedo of global dust aerosols in the shortwave spectrum and relationship to size and iron content. *Atmos. Chem. Phys.* **19**, 15503–15531 (2019).

31. Claquin, T., Schulz, M. & Balkanski, Y. J. Modeling the mineralogy of atmospheric dust sources. *J. Geophys. Res. Atmos.* **104**, 22243–22256 (1999).
32. Moosmüller, H. et al. Single scattering albedo of fine mineral dust aerosols controlled by iron concentration. *J. Geophys. Res.: Atmos.* **117**, n/a–n/a (2012).
33. Journet, E., Balkanski, Y. & Harrison, S. P. A new data set of soil mineralogy for dust-cycle modeling. *Atmos. Chem. Phys.* **14**, 3801–3816 (2014).
34. Nickovic, S., Vukovic, A., Vujadinovic, M., Djurdjevic, V. & Pejanovic, G. Technical Note: High-resolution mineralogical database of dust-productive soils for atmospheric dust modeling. *Atmos. Chem. Phys.* **12**, 845–855 (2012).
35. Zender, C. S., Bian, H. & Newman, D. Mineral Dust Entrainment and Deposition (DEAD) model: Description and 1990s dust climatology. *J. Geophys. Res.* **108**, 4416 (2003).
36. Perlwitz, J. P., Pérez García-Pando, C. & Miller, R. L. Predicting the mineral composition of dust aerosols – Part 1: Representing key processes. *Atmos. Chem. Phys.* **15**, 11593–11627 (2015).
37. Dubovik, O. & King, M. D. A flexible inversion algorithm for retrieval of aerosol optical properties from Sun and sky radiance measurements. *J. Geophys. Res.: Atmos.* **105**, 20673–20696 (2000).
38. Dubovik, O. et al. Application of spheroid models to account for aerosol particle nonsphericity in remote sensing of desert dust. *J. Geophys. Res.* **111**, D11208 (2006).
39. Giles, D. M. et al. An analysis of AERONET aerosol absorption properties and classifications representative of aerosol source regions. *J. Geophys. Res.: Atmos.* **117**, n/a–n/a (2012).
40. Holben, B. N. et al. AERONET—A Federated Instrument Network and Data Archive for Aerosol Characterization. *Remote Sensing Environ.* **66**, 1–16 (1998).
41. Ryder, C. L. et al. Advances in understanding mineral dust and boundary layer processes over the Sahara from Fennec aircraft observations. *Atmos. Chem. Phys.* **15**, 8479–8520 (2015).
42. Müller, D. et al. Mineral dust observed with AERONET Sun photometer, Raman lidar, and in situ instruments during SAMUM 2006: Shape-independent particle properties. *J. Geophys. Res.* **115**, D07202 (2010).
43. Müller, D. et al. Comparison of optical and microphysical properties of pure Saharan mineral dust observed with AERONET Sun photometer, Raman lidar, and in situ instruments during SAMUM 2006. *J. Geophys. Res.: Atmos.* **117**, n/a–n/a (2012).
44. Solmon, F. et al. Dust aerosol impact on regional precipitation over western Africa, mechanisms and sensitivity to absorption properties. *Geophys. Res. Lett.* **35**, L24705 (2008).
45. Strong, J. D. O., Vecchi, G. A. & Ginoux, P. The Climatological Effect of Saharan Dust on Global Tropical Cyclones in a Fully Coupled GCM. *J. Geophys. Res.: Atmos.* **123**, 5538–5559 (2018).
46. Kinne, S. The MACv2 aerosol climatology. *Tellus B: Chem. Phys. Meteorol.* **71**, 1–21 (2019).
47. Russell, P. B. et al. Absorption Angstrom Exponent in AERONET and related data as an indicator of aerosol composition. *Atmos. Chem. Phys.* **10**, 1155–1169 (2010).
48. Caponi, L. et al. Spectral- and size-resolved mass absorption efficiency of mineral dust aerosols in the shortwave spectrum: A simulation chamber study. *Atmos. Chem. Phys.* **17**, 7175–7191 (2017).
49. Ginoux, P., Prospero, J. M., Gill, T. E., Hsu, N. C. & Zhao, M. Global-scale attribution of anthropogenic and natural dust sources and their emission rates based on MODIS Deep Blue aerosol products. *Rev. Geophys.* **50**, RG3005 (2012).
50. Kok, J. F. et al. Contribution of the world's main dust source regions to the global cycle of desert dust. *Atmos. Chem. Phys.* **21**, 8169–8193 (2021).
51. Knippertz, P. & Stuut, J.-B. *Mineral Dust.* (Springer Netherlands, 2014). https://doi.org/10.1007/978-94-017-8978-3.
52. Bevington, P. R., Robinson, D. ~K. K., Blair, J. M., Mallinckrodt, A. J. & McKay, S. Data Reduction and Error Analysis for the Physical Sciences. *Comput. Phys.* **7**, 415 (1993).
53. McConnell, C. L. et al. Seasonal variations of the physical and optical characteristics of Saharan dust: Results from the Dust Outflow and Deposition to the Ocean (DODO) experiment. *J. Geophys. Res.* **113**, 14S05 (2008).
54. Haywood, J. et al. Radiative properties and direct effect of Saharan dust measured by the C-130 aircraft during Saharan Dust Experiment (SHADE): 2. Terrestrial spectrum. *J. Geophys. Res.* **108**, 8578 (2003).
55. Osborne, S. R. et al. Physical and optical properties of mineral dust aerosol during the Dust and Biomass-burning Experiment. *J. Geophys. Res.* **113**, 00C03 (2008).
56. Johnson, B. T. & Osborne, S. R. Physical and optical properties of mineral dust aerosol measured by aircraft during the GERBILS campaign. *Quart. J. Royal Meteorol. Soc.* **137**, 1117–1130 (2011).
57. Ryder, C. L. et al. Optical properties of Saharan dust aerosol and contribution from the coarse mode as measured during the Fennec 2011 aircraft campaign. *Atmos. Chem. Phys.* **13**, 303–325 (2013).
58. Schladitz, A. et al. In situ measurements of optical properties at Tinfou (Morocco) during the Saharan Mineral Dust Experiment SAMUM 2006. *Tellus, Series B: Chem. Phys. Meteorol.* **61**, 64–78 (2009).

59. Formenti, P. et al. Airborne observations of mineral dust over western Africa in the summer Monsoon season: spatial and vertical variability of physico-chemical and optical properties. *Atmos. Chem. Phys.* **11**, 6387–6410 (2011).

60. Müller, T., Schladitz, A., Kandler, K. & Wiedensohler, A. Spectral particle absorption coefficients, single scattering albedos and imaginary parts of refractive indices from ground based in situ measurements at Cape Verde Island during SAMUM-2. *Tellus, Series B: Chem. Phys. Meteorol.* **63**, 573–588 (2011).

61. Haywood, J. M., Francis, P. N., Glew, M. D. & Taylor, J. P. Optical properties and direct radiative effect of Saharan dust: A case study of two Saharan dust outbreaks using aircraft data. *J. Geophys. Res.: Atmos.* **106**, 18417–18430 (2001).

62. Sinyuk, A., Torres, O. & Dubovik, O. Combined use of satellite and surface observations to infer the imaginary part of refractive index of Saharan dust. *Geophys. Res. Lett.* **30**, 1081 (2003).

63. Engelbrecht, J. P. et al. Technical note: Mineralogical, chemical, morphological, and optical interrelationships of mineral dust re-suspensions. *Atmos. Chem. Phys.* **16**, 10809–10830 (2016).

64. Wagner, R. et al. Complex refractive indices of Saharan dust samples at visible and near UV wavelengths: a laboratory study. *Atmos. Chem. Phys.* **12**, 2491–2512 (2012).

65. Eck, T. F. et al. Wavelength dependence of the optical depth of biomass burning, urban, and desert dust aerosols. *J. Geophys. Res.: Atmos.* **104**, 31333–31349 (1999).

66. Otto, S. et al. Atmospheric radiative effects of an in situ measured Saharan dust plume and the role of large particles. *Atmos. Chem. Phys.* **7**, 4887–4903 (2007).

67. Balkanski, Y., Schulz, M., Claquin, T. & Guibert, S. Reevaluation of Mineral aerosol radiative forcings suggests a better agreement with satellite and AERONET data. *Atmos. Chem. Phys.* **7**, 81–95 (2007).

68. Scanza, R. A. et al. Modeling dust as component minerals in the Community Atmosphere Model: development of framework and impact on radiative forcing. *Atmos. Chem. Phys.* **15**, 537–561 (2015).

69. Albani, S. et al. Improved dust representation in the Community Atmosphere Model. *J. Adv. Modeling Earth Syst.* **6**, 541–570 (2014).

70. Mahowald, N. et al. The size distribution of desert dust aerosols and its impact on the Earth system. *Aeolian Res.* **15**, 53–71 (2014).

71. Li, L. & Sokolik, I. N. The Dust Direct Radiative Impact and Its Sensitivity to the Land Surface State and Key Minerals in the WRF-Chem-DuMo Model: A Case Study of Dust Storms in Central Asia. *J. Geophys. Res.: Atmos.* **123**, 4564–4582 (2018).

72. Balkanski, Y., Bonnet, R., Boucher, O., Checa-Garcia, R. & Servonnat, J. Better representation of dust can improve climate models with too weak an African monsoon. *Atmos. Chem. Phys.* **21**, 11423–11435 (2021).

73. O'Sullivan, D. et al. Models transport Saharan dust too low in the atmosphere: A comparison of the MetUM and CAMS forecasts with observations. *Atmos. Chem. Phys.* **20**, 12955–12982 (2020).

74. Myriokefalitakis, S. et al. Reviews and syntheses: the GESAMP atmospheric iron deposition model intercomparison study. *Biogeosciences* **15**, 6659–6684 (2018).

75. Hamilton, D. S. et al. Improved methodologies for Earth system modelling of atmospheric soluble iron and observation comparisons using the Mechanism of Intermediate complexity for Modelling Iron (MIMI v1.0). *Geosci. Model Dev.* **12**, 3835–3862 (2019).

76. Conway, T. M. et al. Tracing and constraining anthropogenic aerosol iron fluxes to the North Atlantic Ocean using iron isotopes. *Nat. Commun.* **10**, 1–10 (2019).

77. Omar, A. H. et al. The CALIPSO automated aerosol classification and lidar ratio selection algorithm. *J. Atmos. Oceanic Technol.* **26**, 1994–2014 (2009).

78. Tesche, M. et al. Ground-based validation of CALIPSO observations of dust and smoke in the Cape Verde region. *J. Geophys. Res.: Atmos.* **118**, 2889–2902 (2013).

79. Wandinger, U. et al. Size matters: Influence of multiple scattering on CALIPSO light-extinction profiling in desert dust. *Geophys. Res. Lett.* **37**, n/a–n/a (2010).

80. Bond, T. C. et al. Bounding the role of black carbon in the climate system: A scientific assessment. *J. Geophys. Res. Atmos.* **118**, 5380–5552 (2013).

81. Adebiyi, A. et al. A review of coarse mineral dust in the Earth system. *Aeolian Res.* **60**, 100849 (2023).

82. Quinn, P. K. et al. Aerosol optical properties during INDOEX 1999: Means, variability, and controlling factors. *J. Geophys. Res.* **107**, 8020–8020 (2002).

83. Weinzierl, B. et al. Airborne measurements of dust layer properties, particle size distribution and mixing state of Saharan dust during SAMUM 2006. *Tellus B: Chem. Phys. Meteorol.* **61**, 96–117 (2009).

84. Efron, B. & Gong, G. A Leisurely Look at the Bootstrap, the Jackknife, and Cross-Validation. *Am. Statistician* **37**, 36–48 (1983).

85. Chernick, M. R. *Bootstrap Methods. Climate Change 2013 - The Physical Science Basis* vol. 53 (John Wiley & Sons, Inc., 2007).

86. Holben, B. N. et al. Aeronet's Version 2.0 quality assurance criteria. in *Remote Sensing of the Atmosphere and Clouds* (eds Tsay, S.-C., Nakajima, T., Singh, R. P. & Sridharan, R.) vol. 6408 64080Q–64080Q (SPIE, 2006).

87. Dubovik, O. et al. Accuracy assessments of aerosol optical properties retrieved from Aerosol Robotic Network (AERONET) Sun and sky radiance measurements. *J. Geophys. Res.: Atmos.* **105**, 9791–9806 (2000).

88. Sinyuk, A. et al. The AERONET Version 3 aerosol retrieval algorithm, associated uncertainties and comparisons to Version 2. Atmospheric. *Measurement Techn.* **13**, 3375–3411 (2020).

89. Engelstaedter, S., Tegen, I. & Washington, R. North African dust emissions and transport. *Earth-Science Rev.* **79**, 73–100 (2006).

90. Kok, J. F. et al. Improved representation of the global dust cycle using observational constraints on dust properties and abundance. *Atmos. Chem. Phys.* **21**, 8127–8167 (2021).

91. Chen, G. et al. Observations of Saharan dust microphysical and optical properties from the Eastern Atlantic during NAMMA airborne field campaign. *Atmos. Chem. Phys.* **11**, 723–740 (2011).

92. Denjean, C. et al. Size distribution and optical properties of African mineral dust after intercontinental transport. *J. Geophys. Res.: Atmos.* **121**, 7117–7138 (2016).

93. Denjean, C. et al. Overview of aerosol optical properties over southern West Africa from DACCIWA aircraft measurements. *Atmos. Chem. Phys.* **20**, 4735–4756 (2020).

94. Clarke, A. D. et al. Size distributions and mixtures of dust and black carbon aerosol in Asian outflow: Physiochemistry and optical properties. *J. Geophys. Res.* **109**, 15S09 (2004).

95. Otto, S. et al. Solar radiative effects of a Saharan dust plume observed during SAMUM assuming spheroidal model particles. *Tellus, Series B: Chem. Phys. Meteorol.* **61**, 270–296 (2009).

96. Meng, Z. et al. Single-scattering properties of tri-axial ellipsoidal mineral dust aerosols: A database for application to radiative transfer calculations. *J. Aerosol Sci.* **41**, 501–512 (2010).

97. Kok, J. F. et al. Smaller desert dust cooling effect estimated from analysis of dust size and abundance. *Nat. Geosci.* **10**, 274–278 (2017).

98. Kaaden, N. et al. State of mixing, shape factor, number size distribution, and hygroscopic growth of the Saharan anthropogenic and mineral dust aerosol at Tinfou, Morocco. *Tellus B: Chem. Phys. Meteorol.* **61**, 51–63 (2009).

99. Fratini, G., Ciccioli, P., Febo, A., Forgione, A. & Valentini, R. Size-segregated fluxes of mineral dust from a desert area of northern China by eddy covariance. *Atmos. Chem. Phys.* **7**, 2839–2854 (2007).

100. Miller, R. L. et al. Mineral dust aerosols in the NASA Goddard Institute for Space Sciences ModelE atmospheric general circulation model. *J. Geophys. Res.* **111**, D06208 (2006).

101. Hurrell, J. W. et al. The Community Earth System Model: A Framework for Collaborative Research. *Bullet. Am. Meteorol. Soc.* **94**, 1339–1360 (2013).

102. Michou, M., Nabat, P. & Saint-Martin, D. Development and basic evaluation of a prognostic aerosol scheme (v1) in the CNRM Climate Model CNRM-CM6. *Geosci. Model Dev.* **8**, 501–531 (2015).

103. Ito, A. & Kok, J. F. Do dust emissions from sparsely vegetated regions dominate atmospheric iron supply to the Southern Ocean? *J. Geophys. Res.: Atmos.* **122**, 3987–4002 (2017).

104. Schmid, B. et al. Evaluation of the applicability of solar and lamp radiometric calibrations of a precision sun photometer operating between 300 and 1025 nm. *Appl. Opt.* **37**, 3923 (1998).

105. Giles, D. M. et al. Advancements in the Aerosol Robotic Network (AERONET) Version 3 database – automated near-real-time quality control algorithm with improved cloud screening for Sun photometer aerosol optical depth (AOD) measurements. Atmospheric. *Measurement Tech.* **12**, 169–209 (2019).

106. Kim, D. et al. Dust optical properties over North Africa and Arabian Peninsula derived from the AERONET dataset. *Atmos. Chem. Phys.* **11**, 10733–10741 (2011).

107. Russell, P. B. et al. A multiparameter aerosol classification method and its application to retrievals from spaceborne polarimetry. *J. Geophys. Res.: Atmos.* **119**, 9838–9863 (2014).

108. Dubovik, O. et al. Variability of Absorption and Optical Properties of Key Aerosol Types Observed in Worldwide Locations. *J. Atmos. Sci.* **59**, 590–608 (2002).

109. Randles, C. A. et al. The MERRA-2 Aerosol Reanalysis, 1980 Onward. Part I: System Description and Data Assimilation Evaluation. *J. Clim.* **30**, 6823–6850 (2017).

110. Weinzierl, B. et al. The Saharan Aerosol Long-Range Transport and Aerosol–Cloud-Interaction Experiment: Overview and Selected Highlights. *Bullet. Am. Meteorol. Soc.* **98**, 1427–1451 (2017).

111. Gliß, J. et al. AeroCom phase III multi-model evaluation of the aerosol life cycle and optical properties using ground- And space-based remote sensing as well as surface in situ observations. *Atmos. Chem. Phys.* **21**, 87–128 (2021).

112. Liu, D. et al. Aircraft and ground measurements of dust aerosols over the west African coast in summer 2015 during ICE-D and AER-D. *Atmos. Chem. Phys.* **18**, 3817–3838 (2018).

113. Denjean, C. et al. Size distribution and optical properties of mineral dust aerosols transported in the western Mediterranean. *Atmos. Chem. Phys.* **16**, 1081–1104 (2016).

114. Adebiyi, A. A. et al. Dust Constraints from joint Observational-Modelling-experiMental analysis – DustCOMM Version 1. Zenodo [Data set]-[Data set] https://doi.org/10.5281/zenodo.2620475 (2019).

115. Adebiyi, A. First release of DustCOMM. Zenodo [Code]-[Code] https://doi.org/10.5281/ZENODO.2620556 (2019).

116. Adebiyi, A. A. et al. DustCOMM_v1 Input Dataset. Zenodo [Data set] https://doi.org/10.5281/ZENODO.2620547 (2019).

117. Adebiyi, A., Huang, Y. & Samset, B. Adebiyi etal: absorption of shortwave radiation by North African dust. https://doi.org/10.5281/zenodo.6406831 (2022).

Acknowledgements

Author contributions

A.A.A. led the research project, which both A.A.A. and J.F.K. designed; B.H.S. provided access to the AeroCom datasets, and Y.H. estimated the single-particle optical properties used in the study. A.A.A. performed the research, analyzed the data, and wrote the paper. All authors discussed the results and provided comments.

Competing interests

The authors declare no competing interests.

Additional information

Supplementary information The online version contains supplementary material available at https://doi.org/10.1038/s43247-023-00825-2.

Correspondence and requests for materials should be addressed to Adeyemi A. Adebiyi.

Peer review information *Communications Earth & Environment* thanks Maria Gavrouzou and the other, anonymous, reviewer(s) for their contribution to the peer review of this work. Primary Handling Editors: Heike Langenberg.

Reprints and permission information is available at http://www.nature.com/reprints

Publisher's note Springer Nature remains neutral with regard to jurisdictional claims in published maps and institutional affiliations.